Analytical Methods

Accepted Manuscript

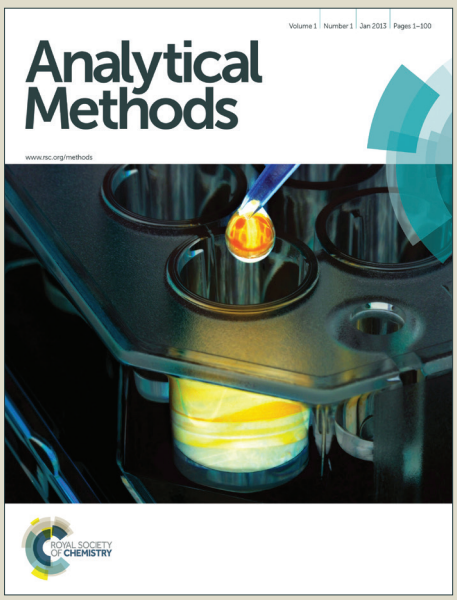

ROYAL SOCIETY OF CHEMISTRY

www.rsc.org/methods

Multianalytical X-Ray based micro-spectroscopic approach for the analysis of carbonates in beachrock cements

Received 00th January 20xx,
Accepted 00th January 20xx

DOI: 10.1039/x0xx00000x

www.rsc.org/

Nikole Arrieta,*[a] Ane Iturregui,[a] Irantzu Martínez-Arkarazo,[a] María Ángeles Olazabal,[a] Xabier Murelaga,[b] Juan Ignacio Baceta [b] and Juan Manuel Madariaga [a]

The molecular micro-characterization and the estimation of the Mg content of the $CaCO_3$ cements, is crucial to define the environmental biophysicochemical conditions in which unusual temperate latitude beachrock formations materialize. To this end, petrographical investigations and a multianalytical micro-spectroscopic approach based on X-ray techniques (Micro-Energy Dispersive X-Ray Fluorescence Spectroscopy (μ-EDXRF), Scanning Electron Microscope-Energy Dispersive X-Ray Spectroscopy (SEM-EDX) and X-Ray Diffraction (XRD)) was at first applied on beachrocks. Such instruments provided the perfect acquaintance for the microscopic inspection of the main metastable $CaCO_3$ cements identified. The Cement Generation 1 (CG1) (5-10 % of the total carbonates) constituted a 15-20 μm thick layer of micron-sized rhombohedral crystals of high magnesium calcite (HMC) ($Ca(Mg)CO_3$) (7.4-12.8 % mol $MgCO_3$). The mineralogy and the trace elements (Si, Al, Na, P, S, Cl, K and seldom Fe) found within that cement, suggest organomineralization activities encouraged by microbiological processes on the first stages of beachrock formation. This is also consistent with the microbiological degradation of the organic matter deposited in the coastal sediments derived from the outfalls of an urban sewage plant. The Cement Generation 2 (CG2) accounted for the 70-85 % of the carbonaceous cements, with isopachous 60-120 μm thick pure fibrous/acicular crystals of orthorhombic aragonite ($CaCO_3$) growing vertically from the CG1 to the pore spaces. The results advocate for a cement precipitation in marine vadose and phreatic subenvironments with an initial saturation of pore-water chemistry promoted by organomineralization activities. The followed multianalytical procedure proved to be a conquering approach for the elemental, molecular and structural micro-stratigraphic characterization of the carbonate cements.

Introduction

Beachrocks come under the arrangement of sedimentary rocks, in which the lithification process involves an early *in-situ* precipitation of intergranular $CaCO_3$ cements in the intertidal zone.[1,2] The composition and the mineralogical habits of the cement generations preserve the entire record of the biophysicochemical conditions that altered the pore-water chemistry inducing the micro-scale cementation.[3,4] Thus, multigenerational cement forms may reflect dissimilar stages to which the rocks were subjected.

The interest in this matter has grown over the last decades due to its socioeconomic impacts, its implications in environmental science, such as green chemistry or the study of global climatic change, and in materials science like innovative engineering approaches for the development of artificial cementation methods based on organomineralization.[5,6]

Essentially, the most common cement constituents in beachrock deposits are the $CaCO_3$ polymorphs calcite and aragonite.[7] These mineral phases differ in their crystal habit but also in their tendency to accept divalent cations other than Ca^{2+} (ionic radii ≈ 1 Å) in solid solution.[8] For instance, calcite presents a rhombohedral structure in which lattice Mg^{2+} cations are frequently incorporated.[2] Depending on the Mg^{2+} content two types of calcite are recognized: low magnesium calcite (LMC) (<3 mol % $MgCO_3$) which in beachrocks is characteristic of meteoric environments, and high magnesium calcite (HMC) (>3 mol % $MgCO_3$) that is more related with marine ambiences.[3,9] Moreover, the existence of HMC is ascribed to a decrease of Ca^{2+} in the dissolved pore water caused by the biologically mediated precipitation of microcrystalline carbonate minerals or organomineralization activities.[10,11] Indeed, several microbial metabolisms could modify the water chemistry by raising locally the level of saturation with respect to carbonate minerals ultimately inducing their precipitation.[12] Consequently, although microbial remains are rarely observed in beachrock cements, the cement mineralogy and concretely, the formation of carbonates with different Mg^{2+}/Ca^{2+} ratios might evidence microbiological activities.[10,13,14] Unlike the calcite, aragonite shows an orthorhombic mineral habit where cations larger than 1 Å such as Ba^{2+}, Na^{+} and specially Sr^{2+} can be accommodated.[2,8] This carbonate phase, is more soluble than calcite and though over time could be replaced by the latter, is the most reported metastable $CaCO_3$ mineral that typically constitutes beachrock deposits in marine environments.[3,7]

The combined use of conventional thin-section petrographic analysis and more detailed microscopy (*e.g.*, stereoscan electron microscopy and fluorescence microscopy) as well as, mineralogical and geochemical studies have proved to be of high potential in carbonate research works.[9] In the scientific papers addressing the subject of beachrocks, thin section petrographic investigations along with Scanning Electron Microscopic (SEM) studies have widely been used to ascertain the crystal micromorphology of the cements.[15-17] Nevertheless, the spectroscopic analyses providing elemental

[a] Department of Analytical Chemistry, Faculty of Science and Technology, University of the Basque Country UPV/EHU, Barrio Sarriena, s/n, 48940 Leioa, Spain. E-mail: nikole.arrieta@ehu.eus; Fax: +34 946013500; Tel: +34 946018298
[b] Department of Stratigraphy and Palaeontology, Faculty of Science and Technology, University of the Basque Country UPV/EHU, Barrio Sarriena, s/n, 48940 Leioa, Spain

and molecular results, have received less attention and there are few works performing multianalytical researches based on these techniques.[1,4,18]

Furthermore, in beachrock studies the wide range of instruments based on X-ray spectroscopy have been mostly restrained to X-Ray Diffraction (XRD) analysis over the carbonate cements.[19-21] Other instruments based on X-rays that have less frequently been used in decreased order are: Energy Dispersive X-Ray Spectroscopy (EDX),[22,23] Energy Dispersive X-ray Fluorescence (EDXRF),[24] and Particle Induced X-ray Emission (PIXE).[25] The μ-EDXRF has importantly contributed to the analysis of geological materials, mainly as a standard instrument for the characterization of the major and selected trace elements in igneous rocks, and in a wide range of geochemical research projects.[26] SEM complemented by the determination of elemental composition via EDX spectroscopy has been used to distinguish different cement generations and resulted fundamental for the chemical characterization of the microcrystalline precipitates and the obtaining of Mg^{2+}/Ca^{2+} ratios.[23] Finally, XRD has proven to be a powerful tool to study polymorphic mineral phases; despite providing a detailed picture of the mineral microstructures, relative percentages of carbonate mineral abundance and Mg contents in ground samples can quantitatively be estimated.[9,27]

The aim of this study was to clarify the molecular and structural micro-stratigraphic sequence (various tens of microns in thickness) of the beachrock cements, with a special interest on the estimation of the Mg content in the micro-scale and thus, the elucidation of the diagenetic environment, the microbiological influence and the biophysicochemical conditions in which the studied beachrocks have materialized at temperate latitudes. The predominant tropical and subtropical distributional evidence of this phenomenon,[28-30] confers a special relevance to the beachrocks formed at higher latitudes, where the seawater tends to be undersaturated with respect to $CaCO_3$ and low rates of evaporation are registered.[31-34] Hence, the beachrock locations studied herein constitute a challenging research field to understand early carbonate diagenesis processes in temperate marine environments.

With the aforementioned background, the present research proposes a multianalytical micro-spectroscopic approach based on the combination of petrographical investigations and other techniques using a point source of X-rays such as, Micro-Energy Dispersive X-Ray Fluorescence Spectroscopy (μ-EDXRF), Scanning Electron Microscope-Energy Dispersive X-Ray Spectroscopy (SEM-EDX) and X-Ray Diffraction (XRD) to study the carbonate cements of beachrock units; a procedure not previously applied in these matrices.

Experimental

Geographical setting and sample acquisition

The studied outcrops emerge in the intertidal zones of Tunelboka cove and Azkorri beach, at a 43° temperate latitude high energy coastline. The emplacements are located 0.5-2 km eastwards the mouth of the Nerbioi-Ibaizabal estuary, adjacent to a semi-enclosed marine bay known as the Abra of Bilbao (Bay of Biscay, Basque Country, North of Spain) (Fig. 1a). The sea cliffs of the area are carved in mixed calciclastic-siliciclastic Eocene turbidites.[35] Although both settings share similar geomorphological features, the beachrocks present higher visible vertical dimensions in Tunelboka cove (up to 12 m), and more extensive longitudes in Azkorri beach (about 1 km long) (Fig. 1b-d).

Within the sedimentary units high amounts of anthropogenic materials were observed. Among them, mainly bricks and slag derived from blast furnace of old steel factories were distinguished. Those materials were transported to the target zones by the marine currents from a submarine disposal area located 6 km north, where more than 25 million tonnes of slag were thrown away during the first half of the 20th century.[36] Moreover, during the industrial development of the mentioned century, the coastal zones also received a high metallic stress coming from the estuarine waters and processing effluents.[37] In addition, Tunelboka cove was the coastal discharge point of the first sewage treatment plant of Bilbao, which started in operation in 1900 and was abandoned in the fifties of the past century. The outfalls contained high amounts of organic matter, bicarbonate (HCO_3^-) and ammonia (NH_3) enriched waters.

Samples were gathered from low to high intertidal locations along the entire disposition of the beaches to find out the mineralogy and the Mg content of the carbonate cements. By the complementary use of a stainless steel chisel and a hammer, 38 samples were collected in the Azkorri beach and 32 in Tunelboka cove.

Sample pretreatment

Based on the materials gathered in both beachrock intertidal locations, 30 μm standard thin sections were produced for mineralogical analyses under polarization microscopy and SEM-EDX. The thin sections were prepared by cutting a thin sliver of rock from the bulk sample with a diamond saw, to be afterwards mounted on a glass slide with epoxy resin and then grounded smooth using progressively finer abrasive grit. Representative 31 slides were created from the samples collected in Azkorri beachrock and 20 from Tunelboka, respectively. Due to the fluorescence attenuation, the corresponding sliver rocks of the thin sections also resulted very functional for the analyses performed by μ-EDXRF and SEM-EDX.

The XRD analyses were selectively carried out over the cements. Those were meticulously removed from the grain surfaces by an electric micro-drill and under a magnification lamp for the proper visualization of the samples. Special care was taken to avoid contamination with beach grains, bioclastic materials and other constituents of the beachrock matrix. Each of the removed samples was mixed with a small amount of silicon, and then, ground and homogenized manually with an agate mortar. In this case, 4 samples from Tunelboka cove and 8 samples from Azkorri beach were analysed.

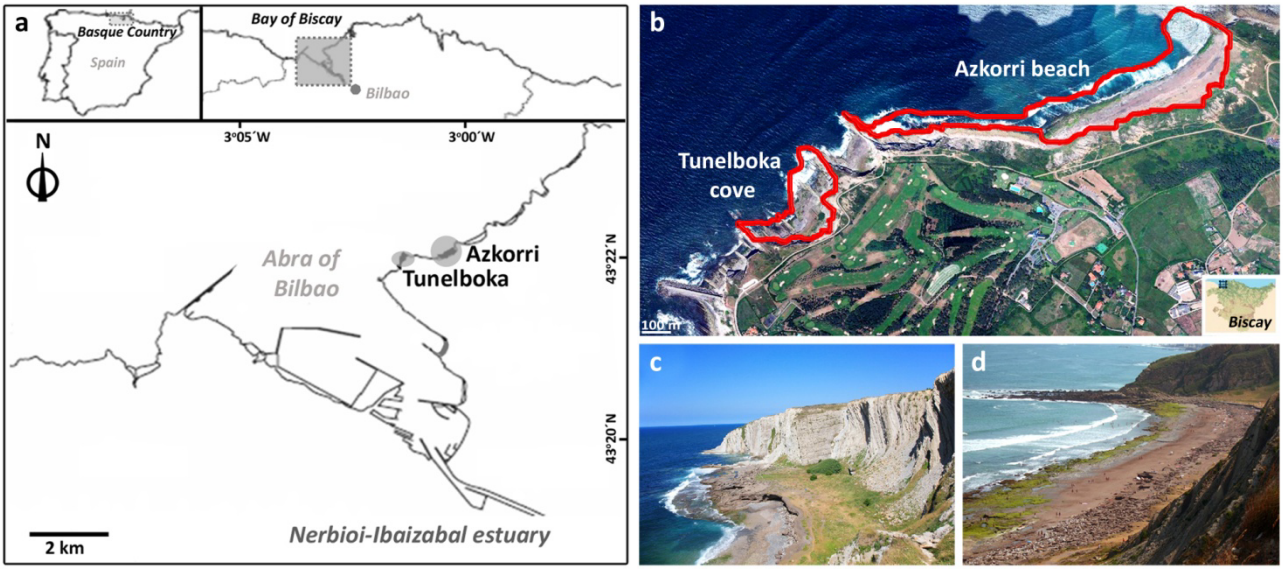

Fig. 1 (a) The geographical location of the studied beachrocks in Tunelboka cove and Azkorri beach. (b) An orthophoto showing the extension of the cemented outcrops. (c) General view of the beachrock deposits in Tunelboka and (d) in Azkorri.

Instrumentation and methodology

Polarization microscopy

The petrographic examinations of the thin sections were conducted under polarization microscopy and constituted the first step prior to the application of the spectroscopic techniques. The optical inspections were aided by a Nikon SMZ 1500 stereo microscope (Tokyo, Japan) which is connected to a digital camera (DS-5 Mpx). Several microphotographs were taken using x2, x4, x8 and x11 focusing lens under polarized light and crossed polarized light (parallel/crossed nicols).

Micro-Energy Dispersive X-Ray Fluorescence Spectroscopy (µ-EDXRF)

In a first screening step the elemental characterization of the samples was performed with the Bruker AG ArtTax portable µ-EDXRF equipment (Berlin, Germany) consisting on a X-ray tube with a molybdenum anode working at maximum voltage of 50 kV and a current of 0.6 mA (maximum power of 35 W). The instrument is provided with an electro-thermally cooled Xflash® detector (5 mm^2). The X-rays are adjusted into line by an Ø 0.65 mm tantalum collimator and the beam diameter in sample surface is of 200 μm^2. The measuring head of the equipment integrates a CCD camera that allows focusing on the sample by a motorized XYZ positioning unit controlled by the computer and gives an 8 mm x 8 mm image of the sample surface.

The detector was daily calibrated with the Cu and Sn Kα lines of a Bruker bronze reference standard. The operating conditions varied between 1000-1500 s at a fix voltage of 50 kV and a current of 0.6 mA. A helium flow was used in order to identify elements with 11<Z<20. This method avoids the use of vacuum conditions. Instrument control, data collection, processing and analysis were performed using the Bruker ARTAX 4.9.13.2 software.

Scanning Electron Microscope-Energy Dispersive X-Ray Spectroscopy (SEM-EDX)

These analyses were performed on the thin sections and the corresponding sliver rocks of the raw samples. Samples were not coated with carbon or gold since they were considered to be partially conductive due to their high metal content.

The mineralogy of the cements was estimated from crystal morphology and the elemental composition confirmed by EDX during SEM analysis. The electron image acquisitions and elemental composition determinations (punctual and element distribution maps) were ascertained by means of a Carl Zeiss NTS GmbH EVO® 40 SEM (Oberkochen, Germany) coupled to an Oxford INCA 350 X-Max EDX system (Oxford Instruments, Oxfordshire, United Kingdom).

SEM images were acquired at high vacuum employing an acceleration voltage of 20-30 kV and 6-13 mm working distance. Magnifications up to x10 000 were reached using a Secondary Electron (SE) detector for image acquisitions. Elemental analyses were performed using an 8.5 mm working distance, a spot-size under 0.5 µm, a 35° take-off angle, 10 scans, an acceleration voltage of 20 kV and an integration time of 50-150 s to improve the signal-to-noise ratio.

In addition to qualitative examinations, the EDX system provided semi-quantitative elemental data of the analysed surfaces. For routine EDX analysis, the detection limits were about 0.1 wt% and taking into account the weight of the lightest (C) and the heaviest (Ca) elements of the matrix, the minimum detection limits varied in the range of 0.02-0.1 $mol.kg^{-1}$. Data analysis was performed with the Oxford INCA Microanalysis Suite 4.3.

X-Ray Diffraction (XRD)

XRD analyses were carried out with a PANalytical Xpert PRO (Toronto, Canada) powder diffractometer, equipped with a

copper tube ($\lambda Cu_{K\alpha media}$= 1.5418 Å, $\lambda Cu_{K\alpha 1}$= 1.54060 Å, $\lambda Cu_{K\alpha 2}$= 1.54439 Å), vertical goniometer (Bragg-Brentano geometry), programmable divergence aperture, automatic interchange of samples, secondary graphite monochromator and PixCel detector. The measurement conditions for the Cu tube were 40 kV and 40 mA, with an angular range (2θ) scanned between 5 and 70°. The data treatment of the diffractograms and the identification of the mineral phases was performed with the PANalytical X`pert HighScore software package in combination with the specific Powder Diffraction File (PDF-2) database (International Centre for Diffraction Data - ICDD, Pennsylvania, USA) and Miller indexing (hkl) of the observed maxima.

The relative proportions of the main carbonate cement forms were semi-quantitatively estimated based on the Relative Intensity Ratio (RIR) values. The carbonates necessarily add to 100 % because the relative proportions of carbonates were only considered, ignoring all the other minerals and amorphous phase of the sample.

Regarding the Mg content, the stoichiometry of the calcites was estimated following the equation of Lumsden (1979),[38] which relates the molar content % $MgCO_3$ of calcite with the displacement of the (104) peak. For that purpose, the silicon (PDF 27-1402) added as an internal standard in the sample to correct the position of reflections was used prior to the application of this equation. The precision of the measurements was ± 0.25 mol %.

Results and discussion

Petrographic analyses

The cemented matrix in both beachrocks consisted of natural components mainly including calcareous siltstone, limestone and sandstone grains, micas, quartzites, feldspars and bioclasts (*e.g.*, oyster shells, fragments of bivalves, equinoderms, gastropods and coralline algae). Besides, high amounts of diverse anthropogenic wastes were observed, but mostly brick fragments, refractory materials, slag and glasses.

The cement generations were well developed and appeared covering completely the surfaces of the different grains with estimated thicknesses of 100-150 µm (Fig. 2a, b). The pore spaces were more restricted in the samples of advanced seaward bands pointing out a marine-phreatic context for the beachrock formation.[1,5,28] However, the irregular thicknesses of the cements covering the beach grains in the samples of the high intertidal zones could indicate vadose environment precipitations (Fig. 2c, d). In fact, the partial desiccation results in an unequal distribution of the pore water that primarily holds near grain contacts by capillary forces.[19,39] The curved pore geometries reflect the meniscus surface of the water caused by surface tension at the time of precipitation.

Based on the most repeated cementation sequence in both beachrocks, two main carbonate cement generations were distinguished: a) covering the sediments as the Cement Generation 1 (CG1) grey micritic crystals, and over those, b) Cement Generation 2 (CG2) of volumetrically more abundant isopachous acicular/needle shaped cements (Fig. 2a-d).

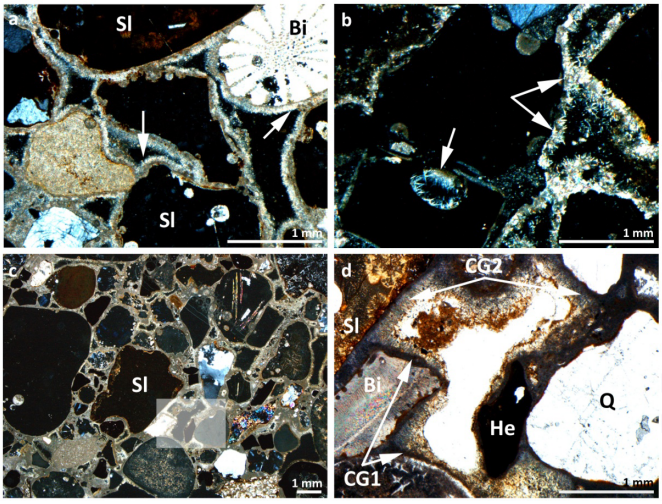

Fig. 2 Thin section microphotographs of the beachrock cements. (a) and (b) Samples from the low intertidal Azkorri beachrock where aragonite acicular crystals are clearly distinguished. (c) General view of a sample from the high intertidal Tunelboka beachrock. (d) Detailed view of the shaded area shown in c, where CG1, CG2 and meniscus-like cements are observed. Images a-c are taken with crossed nicols and d with parallel nicols. In the figures: CG1 Cement Generation 1 (micritic HMC), CG2 Cement Generation 2 (aragonite), He hematite grain, Q quartz, Bi bioclast, Sl Slag.

µ-EDXRF analyses

In order to achieve the elemental composition of the cements, 5 beachrock samples collected at different locations (from low intertidal to onshore) were selected. Fig. 3 shows two examples of the resulting spectra obtained in the cements, and the relative presence of the elements following 10 measurements per sample are reflected in Table 1. Considering that the 200 μm^2 beam diameter at the sample surface is larger than the cement layer thickness, and even the laser was focussed on the cements, some elements corresponding to the adjacent particles could have been detected.

As a first screening step it was an effective instrument to distinguish the major elements of the carbonaceous cements. Overall, the major components of the matrix were Ca, Sr, K, Fe, Mn, Zn and Ti. Ca and Sr have been referred to be representative elements of the cement constituents of beachrock samples.[24] The cements of the sedimentary units are mainly composed of $CaCO_3$ polymorphs and substitutions of Sr for Ca are common in aragonite divalent metal marine carbonates.[2,3]

The two spectra represented in Fig. 3 show an important presence of Sr together with the expected Ca. However, the existence of Sr could also be ascribed to the beach sediments. Moreover, the high presence of Fe, Mn, Zn and Ti might be related to the diverse particulate metallic compounds observed within the matrix that probably reflect the slag wastes dumped to the submarine disposal area.

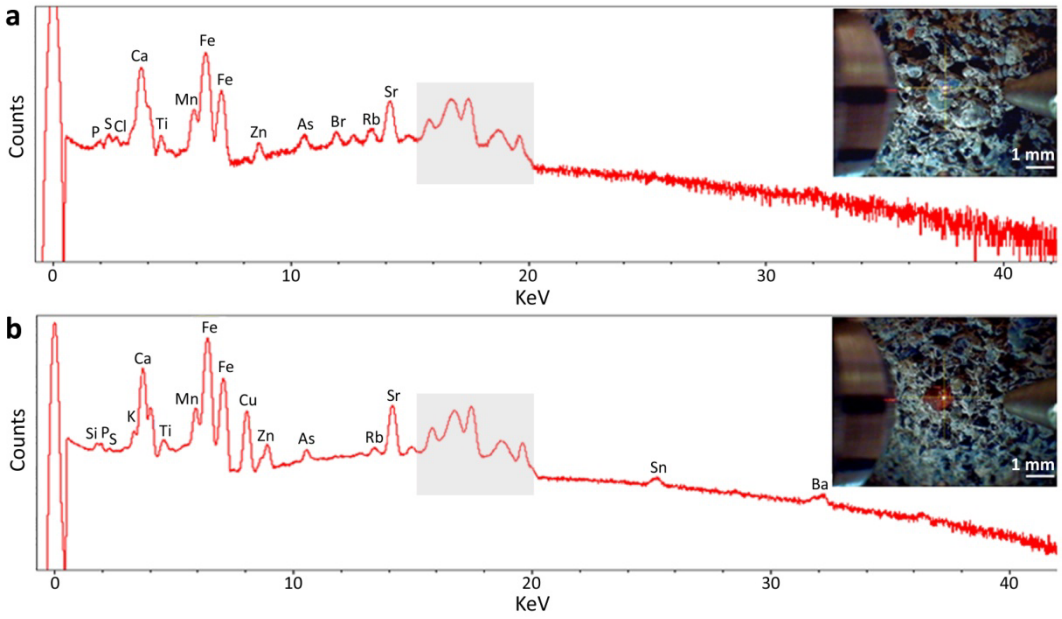

Fig. 3 μ-EDXRF spectra of the cemented sands from (a) Azkorri and (b) Tunelboka. In grey are shaded the energies related with the background of the equipment.

Table 1 The relative presence of the elements by μ-EDXRF analyses in the most representative samples (S) of cemented sands.

Elements	S 15	S 16	S 17	S 36	S 38
Ca	xxx	xxx	xxx	xxx	xxx
Sr	xxx	xxx	xx	xxx	xxx
K	xxx	xxx	xx	xxx	x
Fe	xxx	xxx	xxx	xxx	xxx
Mn	xxx	xxx	xxx	xx	xx
Zn	xxx	xxx	xx	xx	xxx
Ti	xxx	xxx	xx	xxx	x
P	xx	x	x	xx	xx
Si	x	xx	xx	xx	
S		x	xx	xx	x
Cl	xx	xx	x	x	
Cu	xx	x	xx		xx
Pb	x	xx		xx	xx
Br		xx	x	xx	xx
Rb		xx	xx	xx	
Ba	xx	xx	x		xx
V	x	x		x	
Cr		x	x		
Ni		x	x	x	
Co	x	x			x
As		x		x	x
Hg				x	x
Sn	x	xx			
Se			x		
Au		x			
Ga			x		
La					xx

XXX high presence of the elements; XX moderate presence; X low presence

Other elements that appeared moderately were: P, Si, S, Cl, Cu, As, Br, Rb, Sn and Ba. Light elements like P, Si and S were detected using the helium flow coupled to the equipment. However, despite Mg is known to be other Ca replacing element in carbonates giving rise to HMC, its lightness and low amounts did not allowed the detection of this element.

Finally, the minor elements with low or sporadic presence were V, Cr, Ni, Co, Hg, Sn, Se, Au, Ga and La. Many of these elements are infrequent in natural environments and thus, they could have an anthropogenic origin or be associated with scoriaceous materials of the matrix of the cemented sands. Furthermore, elements such as Ga and La, which appeared erratically in the studied materials, are characteristic of rare earths and have also been found in other beachrock samples.[40]

SEM-EDX analyses

The results accomplished by this instrument afforded selective electron image acquisitions and elemental composition determinations of the cements, resulting remarkably valuable for the estimation of the Mg content in the micro-scale.

The crystal morphology of the mineral phases was first ascertained by SEM investigations. The SEM micro-photographs taken over the areas of interest identified in the thin sections, revealed two main cement generations with different crystallographic habits (Fig. 4).

As a general rule, the beach grains were covered by a thin layer of irregular micritic cements, apparently of HMC (CG1) and 15-20 μm thick. These might be considered the nucleation zones for further cement generations.[41] Indeed, above them homogeneously-textured 60-120 μm thick fibrous/acicular aragonite crystals grew vertically filling the pore spaces, which might correspond to the CG2 described in the preceding petrographical analyses.

The existence of the metastable carbonates, HMC and aragonite, suggests that the precipitation of the beachrock cements arose in a marine context.[7] Moreover, the micron-sized irregular rhombohedral crystals (CG1) might be indicative of the rapid super-saturation of pore waters produced by biochemical processes in the first stages of beachrock

formation.[14] In microbial induced precipitates, the lattice incorporation of Mg^{2+} in calcite may be accompanied by a modest relative change in the activity product of Ca^{2+} and CO_3^- ions. The smaller ionic radius of Mg^{2+}, relative to Ca^{2+}, causes lattice distortion at the edge of the growing crystal, stopping growth at the edge and ultimately leading to the elongation of the crystal in the *c-axis* direction.[8] Therefore, when the Mg^{2+}/Ca^{2+} ratios of the solution are high (as in marine conditions), calcite and aragonite crystals are prevented from growing sideways, so that from rhombohedral to fibrous/acicular elongate crystals are common.[42]

Furthermore, most of the different cement thicknesses found were in accordance with the locations of the samples in the intertidal zones. Hence, the samples placed at advanced seaward bands presented lengthened crystals, reinforcing that the precipitation occurred in a marine ambience (Fig. 4a-c).

Complementary to those data and pursuing the determination of the elemental composition associated to each of the cement generations (CG1 and CG2), EDX point analyses (10 measurements per cement) were performed.

This instrument provided more accurate elemental data in the micro-scale due to the high magnifications (up to x10 000) reached using the SE detector for image acquisitions.

Overall, in decreasing order of abundance, CG1 cements contained an average of: O (55 %), C (20 %), Ca (10 %), Mg (8 %), Si (3 %) and traces (<1 %) of Al, Na, P, S, Cl, K and seldom Fe. These results supported the presence of HMC and the existence of such traces was likely related to an involvement of mineral fragments by organomineralization processes of bacteria or algae organisms.[22,23,43] With regard to the CG2 cements, they comprised on average O (50 %), C (38 %), Ca (11 %) and traces of Na and Cl (<1 % each), probably related to marine salt depositions in the pore spaces.

Fig. 4c shows a SEM image where a bioclast (distinguished by its soft appearance) is covered by the two cement forms: a first ~20 µm thick micritic layer of presumably HMC (CG1), overlaid by elongated aragonite acicular crystals which correspond to the CG2. Several point spectra were taken over each area; however, in Fig. 4d only three EDX point spectra for each zone are represented. Thus, in the EDX profile, spectra 1-3 are related to the elemental composition of the shell (bioclast), spectra 6-8 to the CG1 and 16-18 to the CG2. Note the purest composition of the aragonite cements (CG2) which aside from C, O and Ca only presented traces of Cl, against the composition of the micritic HMC (CG1), where Mg, Si and traces of Na were also observed in addition to C, Ca and O.

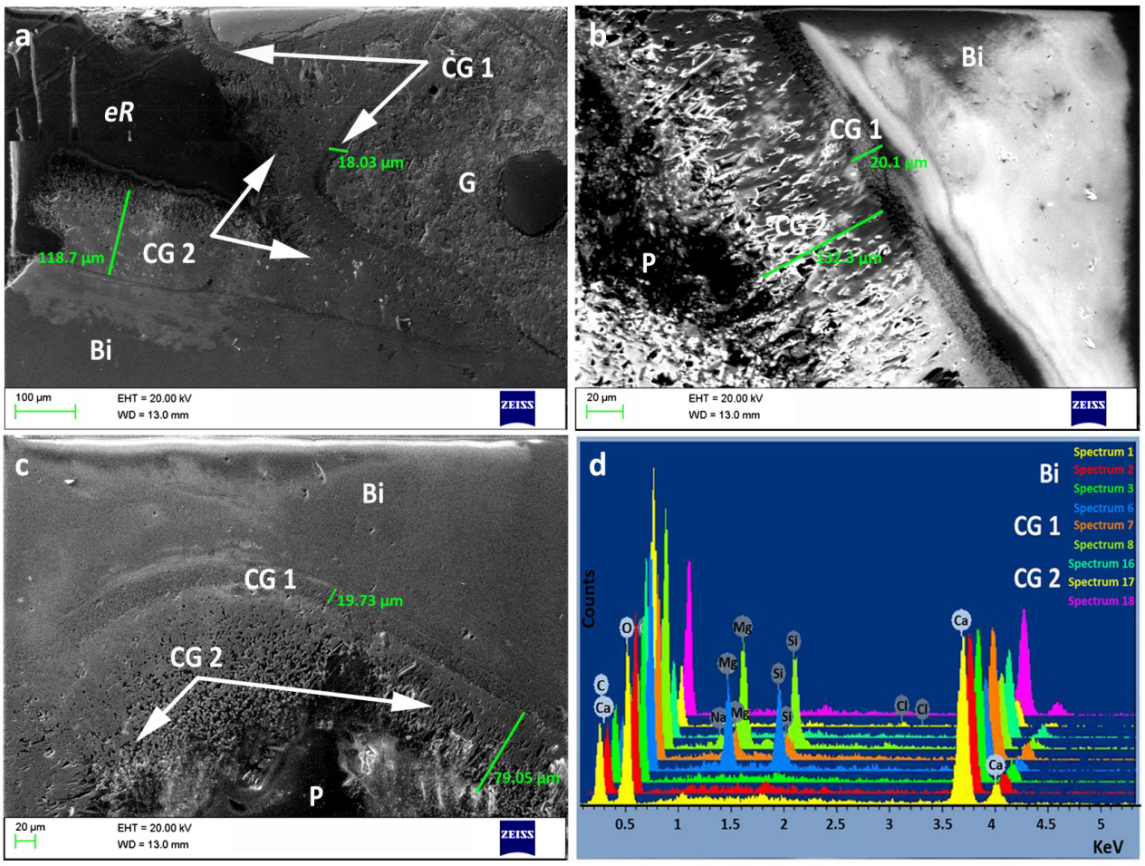

Fig. 4 SEM micro-photographs showing the different morphologies of the cements. (a) and (b) Samples of advanced seaward bands of Tunelboka and Azkorri beachrocks showing the bordering areas of grains and bioclasts covered by the cement generations. (c) A SEM image of a sample from the high intertidal zone showing a bioclast covered by CG1 and CG2. (d) The EDX point spectra acquired over each area of interest shown in (c). G grain, Bi bioclast, CG1 and CG2 Cement Generation 1 and 2, P pore-space, eR epoxy resin.

Apart from that, the % element values of each EDX point spectra taken over the cement generations were transformed in mol.kg^{-1} units and a Mg/Ca ratio was calculated for CG1. Table 2 shows the acquired elemental data and the Mg/Ca ratio calculated for the CG1 observed in Fig. 4c.

The SEM-EDX investigations performed selectively over the CG1 determined the presence of Mg and an average value of 2.05 ± 0.96 mol.kg^{-1} of Mg was estimated. The obtained Mg/Ca ratio varied between 0.19-1.85. Although in some of the point spectra the ratio values were slightly lower than they were supposed to be, most of them showed higher values than those referred for the LMC and met the criteria to be considered as HMC precipitates from marine ambiences with a salinity of 32 ‰.[3,9] Moreover, some authors have attributed the relative low Mg contents to the effect of low temperature, as the Mg content of biologically fixed calcites increases with increasing temperature.[44] Furthermore, other authors consider ordinary to find such variable Mg/Ca ratios in the carbonate micro-scales when are precipitated by organomineralization activities.[10,45]

Table 2 EDX point spectra analysis (mol.kg^{-1}) over a shell and the cement generations.

Point Spectra		C	O	Na	Mg	Si	Cl	Ca	Mg/Ca ratio
Shell	1	15.9	38.4					4.86	
	2	12.9	40.6					4.89	
	3	16.4	38.6					4.64	
	4	17.0	37.3					5.00	
	5	17.3	37.4					4.84	
CG1	6	14.5	38.1		2.66	1.83		2.53	1.05
	7	16.4	38.5		0.88	0.45		3.82	0.23
	8	19.2	35.4	0.34	2.79	1.88		1.84	1.51
	9	19.1	35.5		2.40	1.54	0.10	2.41	1.00
	10	18.2	37.8		0.72	0.44		3.68	0.19
	11	15.9	38.1		0.95	0.70		3.91	0.24
	12	19.6	33.2		2.92	2.16	0.18	2.38	1.23
	13	17.2	35.9		2.27	1.68		2.90	0.78
	14	18.2	34.7		3.39	2.38	0.13	1.83	1.85
	15	18.1	36.5		1.56	1.09		3.27	0.48
CG2	16	37.0	27.2					2.99	
	17	49.2	22.6				0.12	1.09	
	18	20.2	38.6					3.47	
	19	24.6	35.6					3.39	
	20	28.7	32.1					3.52	
	21	59.3	16.5				0.12	0.49	
	22	17.5	39.3					4.01	
	23	45.0	25.2				0.10	1.31	
	24	22.4	33.9					4.71	
	25	22.6	35.2					4.14	

CG1 Cement Generation 1 (HMC); CG2 Cement Generation 2 (aragonite)

Fig. 5 reflects another example of a microscopic area where EDX analyses were carried out. In the false colour image that was performed over the SEM image, the Mg energies are represented in blue and can be clearly distinguished in the CG1 overlaying the grain surfaces (Fig. 5a). In the EDX element distribution maps there is a noticeable presence of Ca and C in the cement forms that appear covering the grain surfaces. The grain of the left could be a silicate composed of Ca, Mg and Al, while the grain on the right might be a silicate with minor traces of Al, maybe an aluminosilicate. Over the electron image a 232 µm transect from the grain of the right (the possible aluminosilicate) to the acicular crystals of the CG2 was performed. From all those data it can be inferred that Ca is present in both CG1 and CG2, while Mg is only evidenced in CG1. There are apparently major contents of C in the CG1, which could be related to the first pore saturation state for the precipitation of carbonates and the multiple nucleation zones of the first cement generation. Furthermore, between the CG1 and the CG2 it appears to be a transition zone, noticeable by the lack of signals of Ca and O, and a slight presence of C.

Additionally, Fig. 5b represents the distributions of diverse elements through the performed transect, where the yellow lines (which appear transversal to the bars of the elements studied) mark the external limit of the grain. The graphic demonstrates that the siliciclastic grain is first overlaid by a cement form of 20 µm where the Mg is present (green bars) and also Ca (magenta bars) but with a lower intensity than in the subsequent cement generation. Moreover, the Si remains distinguished within the CG1, could correspond to the organomineralization processes cited before. After that, the CG2 is mainly composed of Ca.

XRD Analyses

This technique has been widely used on the subject of beachrocks to distinguish between meteoric and marine cements, so as to determine the Mg contents over the calcite cement forms traduced in estimated ranges for those cement generations, or even to detect other mineral phases of the framework grains. [4,19,21,32] The SEM-EDX analyses carried out revealed selectively the existence of Mg in the CG1. However, in the mechanical micro-extraction step of the cements to perform XRD analyses, it was physically not possible to extract solely the CG1 and both cement forms were removed from the grain surfaces. Therefore, aside from the molecular identification of the mineral phases detected in both cement generations, relative percentages of carbonate mineral abundance and Mg contents in ground samples were quantitatively estimated by the XRD analyses. These results confirmed the data provided by the preceding techniques with the subsequent implications regarding the possible role of the biological processes involved in the formation of beachrocks.

On the whole, the molecular phases identified were mainly carbonates and silicates. In Fig. 6 are shown two diffractograms where some of the minerals detected within the beachrock cements can be observed.

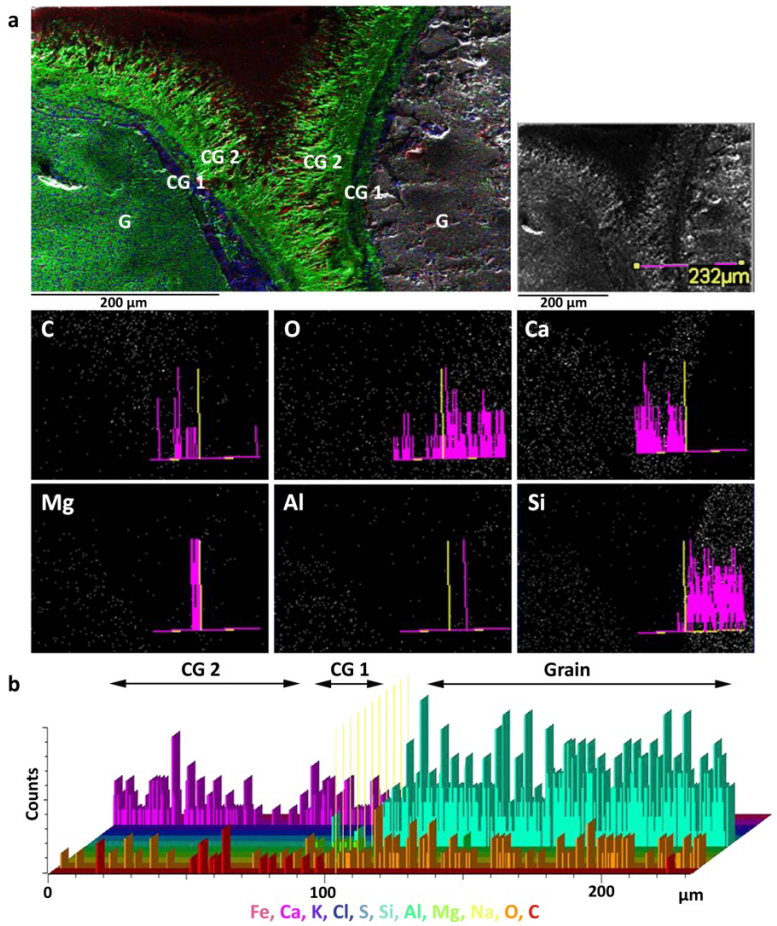

Fig. 5 (a) False colour image performed over the area of interest where the energies of Ca are represented in green, of the Mg in blue and of the C in red. Two grains (G) appear overlaid by CG 1 and CG 2. On the right, an electron image with the performed transect over the area of interest and below, the element distribution maps showing the counts of the detector at each point for each element (magenta bars). The yellow line marks the end of the grain of the right. (b) The element distribution through the performed transect where the composition of the grain, the CG 1 and the CG 2 are distinguished.

Among the silicates, customarily trigonal quartz (SiO_2) with its main peak at (011) was found (PDF 85-798) and in some samples signs of phyllosilicates were also identified; such compounds could form part of the natural sandstone matrix.

Besides, in several samples akermanite-gehlenite ($Ca_2Mg(SiO_7)$-Ca_2Al ($AlSiO_7$)) silicate tetragonal series distinguished by the maximum (211) peak were detected. These mineral phases could be assumed to be part of the slag of anthropogenic origins. Indeed, the blast furnace final slag is made from the meltdown liquid of sinter, lump, coke and flux at high temperature, and can be approximately considered a mixture of the four oxides, SiO_2, Al_2O_3, CaO, and MgO, thus akermanite and gehlenite are commonly derived from those processes.[46,47] Furthermore, occasionally, signs of cristobalite (SiO_2) appeared to be found. This mineral is a polymorph of silica usually formed at high temperatures, so it could also be related to the formation of the slag.

It must be mentioned that these silicate mineral phases were not probably related to the cements. Some of these silicate inclusions among the carbonates could possibly be ascribed to the organomineralization activities or the microorganisms producing carbonate sub-products. Nonetheless, most likely most of them might be related to impurities coming from the micro-mechanical extraction of the cements from the framework grains.

The presence of the carbonaceous minerals previously identified by the petrographic inspections and SEM-EDX investigations was confirmed with XRD analyses. This technique provided a straightforward way to distinguish between the two polymorphs of $CaCO_3$, aragonite and calcite. The highest intensity peaks of both mineral phases are shown at different positions in the diffractograms, and the general view of the two patterns is different, what makes analysis of mixtures more challenging.

Generally the diffractograms were dominated by peaks related with orthorhombic aragonite ($CaCO_3$), detected by its maximum peak (111) at relatively small °2θ and several lesser peaks (Fig. 6a). The identification of aragonite was performed by the standard PDF 76-606 pattern. Furthermore, trigonal calcite ($CaCO_3$) with different amounts of Mg was distinguished by its booming (104) peak a bit to the right of the aragonite large peak and by a few comparatively small other peaks (PDF 5-586). The calcite (104) peak is so robust that it is typically larger than the aragonite (111) peak, even in a mixture that is 75 % aragonite. Thus, comparison of the most intense peaks becomes a potentially misleading endeavour.

Moreover, rhombohedral magnesium calcites or HMC ($Ca(Mg)CO_3$) were also observed (PDF 89-1306). The peaks corresponding to the Mg-calcites are unusually asymmetrical and show shoulders towards higher $^{o}2\theta$ angles of the peak (104) (towards smaller unit cell sizes) (see Fig. 6a). As mentioned before, since the size of the cations Ca^{2+} and Mg^{2+} is different, the presence of magnesium in the structure of the calcite causes its cell parameters to be a bit smaller affecting slightly the peak position. Such an asymmetry is generally interpreted to represent magnesian calcite that is more Mg-rich than the average.[48] Additionally, other not well crystallized, disordered and and possibly bordering on an amorphous crystal structure, thus not diffracting X-rays well, were also detected. The origin could be attributed either to amorphous carbonate cement forms, to the presence of remainders of natural organic matter, or to a glassy phase contained in the slag.[49]

The relative percentages of the carbonate mineral abundance in the cements was estimated based on the Relative Intensity Ratio (RIR) values. In both beachrocks, the majority of the precipitates were related to the aragonite mineral phase, accounting for the 70-85 % of the total carbonates, whereas calcite cement forms (with variable amounts of Mg) referred to the 5-12 % and the high magnesium calcites to the 5-10 %. Those values were in accordance with the relative thicknesses observed under SEM (10-20 µm for the CG1 and 60-120 µm for the CG2). Thus, the percentage variances of the carbonates relative proportions, could also account for the differences of the cement thicknesses observed by the previous techniques.

Based on the crystal morphologies and the elemental compositions observed in the preceding analyses, it was identified that the CG1 was mainly composed of rhombohedral micritic crystals of HMC and the CG2 of needle-shaped acicular crystals of aragonite. Therefore, the proportion of the calcites (with variable amounts of Mg) found in the XRD analyses could probably be related to the exposition of the cements to weathering processes caused by meteoric waters. The external side of the aragonite cements is exposed to the pore-spaces in which some reprecipitation occur, when marine cements (such as aragonite) are long time exposed to meteoric conditions, tend to partially dissolve and be replaced by calcites with lower concentration of Mg.[2,3,8] This fact was corroborated in the samples from the high intertidal zones (more exposed to the weathering processes) where, in some cases the percentages of aragonite decreased up to 53-56 %, and the abundance of calcites increased to 40-43 % (see Fig. 6b). Hence, in the cements of the high intertidal vadose ambiences it was observed an important influence of the exposition of the beachrocks to the meteoric conditions. Indeed, in the petrographic inspections of the samples located in the high intertidal zones meniscus-like crystal morphologies were more frequently observed, reinforcing such meteoric influence.

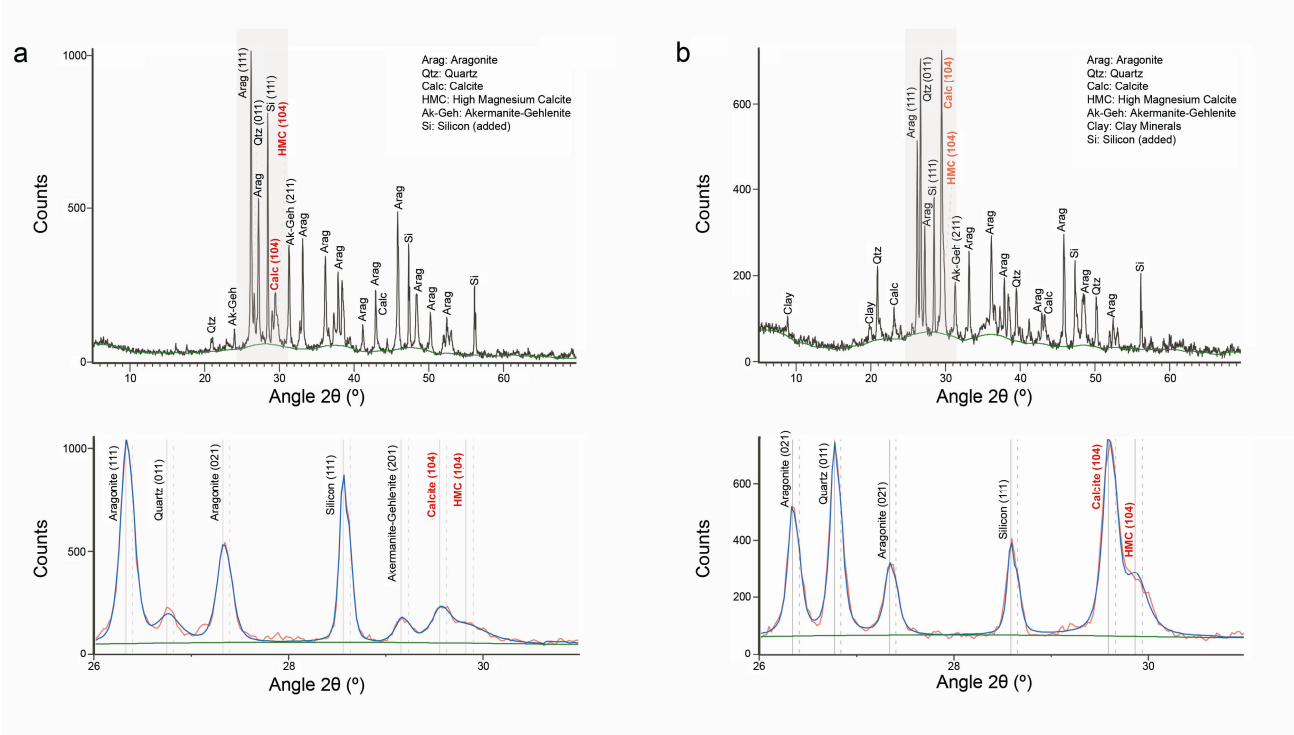

Fig. 6 XRD diffractograms of the beachrock cements including the maximum (hkl) Miller index of the different mineral phases detected and the corresponding 26-31° 2θ angular range where, the profile fitting (blue line) and the experimental XRD data (red line) are shown along with the main peaks for aragonite, calcite, HMC, quartz, akermanite-gehlenite, clay minerals and the added silicon. In the 26-31º 2θ regions, vertical solid and discontinuous lines are the Kα1 and Kα2 components of each peak, respectively. (a) An example of the mineral phases detected in a sample from the Azkorri beachrock with 9 mol % $MgCO_3$ in the HMC. (b) An example of the mineral phases detected in a sample from the high intertidal zone of Tunelboka beachrock with 12.8 mol % $MgCO_3$ in the HMC. For easier viewing reflections are labelled in selected scans only.

With reference to the Mg content, it was applied the equation of Lumsden (1979) of calculating the average molar content % $MgCO_3$ of the calcites based on (104) peak position. As mentioned before, the presence of high magnesian calcites is manifested by a broad shoulder or an asymmetry on the side of the highest 2θ angular range of the maximum (104) peak position of the calcite. Therefore, an amplification of the 26-31° 2θ angular range facilitates the observation of the maximum calcite peak (104), the corresponding shoulder of the magnesian calcites (104), and the maximum peak (111) of the silicon standard against the displacement is corrected (see Fig. 6a, b down). In each particular diffractograms the displacement was calculated by measuring the position of the maximum of silicon and correcting it with respect to the theoretical position thereof. In the studied samples, the corrections were of the order of 0.11° 2θ.

The Mg content for the calcites and the high magnesian calcites was estimated. Based on the data collected of the beachrock samples from both emplacements, the Mg contents of the calcites varied in a range of 1.6-3.1 mol % $MgCO_3$, and in the high magnesium calcites between 7.4-12.8 mol % $MgCO_3$. For instance, in the sample from the Azkorri beachrock cements shown in Fig. 6a, 3.1 mol % $MgCO_3$ in the calcites and 9 mol % $MgCO_3$ in the HMC were estimated. In this case, the calcite 104 reflection has no significant shoulder, but displays a strong asymmetry that is typical for biologically mediated Mg-rich calcites.[48] However, the relatively high Mg-content of the sample from Tunelboka beachrock reflected in Fig. 6b, with 1.9 mol % $MgCO_3$ in the calcites and 12.8 mol % $MgCO_3$ in the HMC is consistent with the distinct shoulder displayed by the calcite 104 reflection towards higher angles 2-theta. Both the marked shoulders and curve asymmetry towards high 2-theta indicate the presence of more magnesium rich Mg-calcite (low-Mg-calcite will have asymmetry towards the low 2-theta side).

Although the Mg values in the calcites from the Azkorri beachrock were slightly lower than the ones observed in Tunelboka, the variation observed in the % mol $MgCO_3$ contents of the calcites might be ascribed to the heterogeneity of such cements possibly biologically mediated. The higher Mg contents registered in Tunelboka cove might reflect more active organomineralization processes that could be explained based on the high quantities of organic matter accumulating in that area from the sewage outfalls during half a century. Indeed, the important point is that the presence and abundance of organic matter is usually linked to microbial proliferation during organic matter degradation.[10]

Conclusions

The existence of beachrocks at temperate and cold latitudes deserves a special interest to corroborate that these peculiar geological units are not exclusively linked to specific tropical climate regions or evaporation processes. Further factors like the alteration of the biophysicochemical conditions by intense pollution episodes may also raise locally the pH of the microenvironment favouring the carbonate precipitation.

The followed multianalytical procedure based on X-ray techniques has proven to be a conquering approach for the elemental, molecular and structural micro-stratigraphic characterization of the carbonate cements. The separate application of the techniques or the use of a limited subset of the instruments would lead to a failure in the detection of some compounds of the cements. For instance, though the μ-EDXRF contributed in the characterization of the major elements of the cements, also revealed other elements linked to the sediments because the laser spot at the sample surface was of 200 μm^2 and the overall size of both cements was 100-150 μm. The destructive analyses performed over the cements by XRD provided complementary information through the estimation of the relative proportions of the carbonate cements and the % mol $MgCO_3$ in the calcites. Nevertheless, the latter technique was not useful to afford non-destructive specific measurements in the different morphologies of the microcrystalline cements, whilst the EDX analyses were directly conducted in the target zones.

In this context, although it is actually beyond the scope of the current manuscript, to complementary support the hypothesis suggested in this work which advocates for an initial microbial mediation on the precipitation of carbonates, the application of other analytical procedures based on micro-Raman spectroscopy, ICP-MS or Stable Isotopic Analysis (*e.g.* $\delta^{13/12}$ C and $\delta^{18/16}$ O) performed selectively on the cements, could helpfully contribute in forthcoming works on the selective identification of the minerals composing the cement generations, the determination of the Mg content and the microbiological diagenetic influence on beachrock formation.

The combined use of the applied analytical tools successfully lead to conclude that in the studied unusual temperate latitude formations, as in other referred beachrocks, the main mineral phases detected within CG1 and CG2 were metastable $CaCO_3$ minerals. Considering the mineralogy of the CG1 (HMC) and the diverse trace elements (Si, Al, Na, P, S, Cl, K and seldom Fe) found within this cement, it could be inferred a microbiological influence in the first stages of the studied beachrock formations. Several microbial metabolic pathways (*e.g.*, photosynthetic carbon fixation by cyanobacteria, hydrolysis of urea or sulphate reduction) alter the geochemical environment conditioning carbonate precipitation.[12,45] Those biologically mediated carbonates usually show different Mg^{2+}/Ca^{2+} ratios in beachrock deposits.[13,22,41,50] Accordingly, this cement would have been the result of the microbiological degradation of the organic matter deposited in the coastal sediments derived from the floating suspended solids from the urban sewage waters. Such fermentable materials were probably decomposed by the cited metabolic pathways leading to organomineralization activities producing calcites with different amounts of % mol $MgCO_3$ in their structures. Besides, the isopachous rims and the purity of the aragonite crystals composing the CG2, suggests that the precipitation of these cements occurred in marine environment under physicochemical conditions when a deceleration of carbonate precipitation in saturated water-filled pores took place.

To conclude, it must be highlighted that the conjunction of the identified carbonate cements and the fact that the samples from advanced seaward bands presented more elongated crystals advocate for cement precipitations in marine phreatic subenvironments with an initial saturation of pore-water chemistry promoted by organomineralization activities. However, the presence of meniscus-like features and the increase in the relative proportions of the calcites found by XRD in the samples of the high-intertidal zones indicated that the precipitation in such regions possibly occurred in marine-vadose ambiences, with the consequent exposition to weathering processes or meteoric waters. Thus it might not be underestimated to find further carbonate cements related to meteoric environments.

Finally, it must be mentioned that this work has opened a new line of research in the direction of the identification of microbiological traces and biomarker compounds in the cements to have even more specific data of the first stages of the cementation processes probably ascribed to biological mediated activities.

Acknowledgements

This work has been financially supported by the project PRIACE from the Spanish Ministry of Economy and Competitiveness (MINECO) and the European Regional Development Fund (FEDER) (ref. CTM2012-36612). Authors are grateful to the technical support provided by the Raman-LASPEA laboratory and to the General X-Ray Service: Unit of Rocks and Minerals, of The Advanced Research Facilities of the SGIker (UPV/EHU, MICINN, GV/EJ, ERDF and ESF). N. Arrieta acknowledges the UPV/EHU for the call for aid for the recruitment of recent doctors to their integration in postdoctoral training programs of the Vice-Chancellor office of Research of the UPV/EHU. A. Iturregui is grateful to the Basque Government for her pre-doctoral fellowship.

References

1 M. M. Vieira and L. F. De Ros, *Sediment. Geol.*, 2006, **192**, 207-230.
2 N. -M. Hanken, K. Bjorlykke and J. K. Nielsen, in *Petroleum Geosciences: From Sedimentary Environments to rock Physics*, ed. K. Bjorlykke, Springer-Verlag, Berlin, 2010, pp. 141-200.
3 E. Gischler and A. J. Lomando, in *Geochemical Sediments and Landscapes*, ed. D. J. Nash and S. J. McLaren, Wiley-Blackwell, 2007, pp. 365-390.
4 A. E. Erginal, N. G. Kıyak, M. Z. Ozturk, M. Avcioglu, M. Bozcu and E. Yiğitbaş, *Sediment. Geol.*, 2012, **243-244**, 148-154.
5 R. F. McLean, in *Encyclopaedia of Modern Coral Reefs: Structure, Form and Process*, ed. D. Hopley, Springer, Dordrecht, London, 2011, pp. 107-111.
6 M. I. Vousdoukas, A. F. Velegrakis, M. Paul, C. Dimitriadis, E. Makrykosta and D. Koutsoubas, *Cont. Shelf Res.*, 2012, **48**, 100-109.
7 T. Danjo and S. Kawasaki, *Geotech. Geol. Eng.*, 2014, **32**, 215-246.
8 J. W. Morse, R. S. Arvidson and A. Lüttge, *Chem. Rev.,* 2007, **107**, 342-381.
9 E. Flügel, in *Microfacies of Carbonate Rocks. Analysis, Interpretation and Application*, second ed., Springer-Verlag, Berlin Heidelberg, New York, 2010, pp.80-385.
10 H. Hillgärtner, C. Dupraz and W. Hug, *Sedimentology*, 2001, **48**, 117-131.
11 C. Dupraz, R. P. Reid, O. Braissant, A. W. Decho, R. S. Norman and P. T. Visscher, *Earth Sci. Rev.*, 2009, **96**, 141-162.
12 R. Riding, *Sedimentology*, 2000, **47**, 179-214.
13 W. E. Krumbein, *Geomicrobiol.* J., 1979, **1**, 139-203.
14 G. E. Webb, J. S. Jell and J. C. Baker, *Sediment. Geol.,* 1999, **126**, 317-334.
15 A. V. Ferreira-Junior, T. C. M. Araújo, M. M. Vieira, V. H. Neumann and M. N. Gregorio, *Geociencias*, 2011, **30**, 545-559.
16 S. K. Kumar, N. Chandrasekar, P. Seralathan and J. D. Sahayam, *J. Earth Syst. Sci.*, 2012, **121**, 733-745.
17 I. M. Ghandour, H. A. Al-Washmi, R. A. Bantan and M. M. Gadallah, *Arab. J. Geosci.*, 2014, **7**, 355-365.
18 R. Ravisankar, P. Eswaran, A. Rajalakshmi, A. Chandrasekaran, K. K. Thillaivelavan and B. Dhinakaran, *Adv. Appl. Sci. Res.*, 2012, **3**, 95-102.
19 D. Kneale and H. A. Viles, *Sediment. Geol.*, 2000, **132**, 165-170.
20 I. P. Swainson, *Am. Mineral.*, 2008, **93**, 1014-1018.
21 R. Ravisankar, A. Chandrasekaran, S. Kalaiarsi, P. Eswaran, C. Rajashekhar, K. Vanasundari and A. Athavalee, *Arch. Appl. Sci. Res.*, 2011, **3**, 77-84.
22 U. Neumeier, *Sediment. Geol.*, 1999, **126**, 35-46.
23 A. E. Erginal, Y. L. Ekinci, A. Demirci, M. Bozcu, M. Z. Ozturk, M. Avcioglu and E. Oztura, *Sediment. Geol.*, 2013, **294**, 294-302.
24 R. Ravisankar, P. Eswaran, K. Vijay Anand, A. Rajalakshmi, M. V. R. Prasad, K. K. Satpathy, C. Rajashekhar and A. Athavale, *Nucl. Sci. & Tech.*, 2009, **20**, 93-98.
25 R. Ravisankar, A. Rajalakshmi, P. Eswaran, V. Meenakshisundaram, V. Gajendiran, E. Manikandan, P. Magudapathy, B. K. Panigrahi and K. G. M. Nair, *Int. J. PIXE*, 2007, **17**, 193-203.
26 M. West, A. T. Ellis, P. J. Potts, C. Streli, C. Vanhoof and P. Wobrauschek, *J. Anal. At. Spectrom.*, 2014, **29**, 1516-1563.
27 H. Pesenti, M. Leoni and P. Scardi, Z. Kristallogr. Suppl., 2008, **27**, 143-150.
28 D. Spurgeon, J. R. A. Davis and E. A. Shinn, Mar. Geol., 2003, **200**, 19-29.
29 R. F. Amaral and F. H. R. Bezerra, *J. Coastal Res.*, 2006, 39, 270-274.
30 M. I. Vousdoukas, A. F. Velegrakis and T. A. Plomaritis, *Earth Sci. Rev.*, 2007, **85**, 23-46.
31 D. Rey, B. Rubio, A. M. Bernabeu and F. Vilas, *Sediment. Geol.*, 2004, **169**, 93-105.
32 F. M. P. Howie, in *Geoscience in South-West England*, ed. Ussher Society, 2009, 12, pp. 85-94.
33 A. Iturregui, N. Arrieta, J. I. Baceta, X. Murelaga, M. Olazabal, I. Martínez-Arkarazo and J. M. Madariaga, *Anal. Methods*, 2014, **6**, 8247-8257.
34 N. Arrieta, N. Goienaga, I. Martínez-Arkarazo, X. Murelaga, J. I. Baceta, A. Sarmiento and J. M. Madariaga, *Spectrochim. Acta A*, 2011, **80**, 55-65.
35 S. Ortiz, L. Alegret, A. Payros, X. Orue-Etxebarria, E. Apellaniz and E. Molina, *Mar. Micropaleontol.*, 2011, **78**, 1-13.
36 A. Borja, I. Tueros, M. J. Belzunce, I. Galparsoro, J. M. Garmendia, M. Revilla, O. Solaun and V. Valencia, *J. Environ. Monit.*, 2008, **10**, 453-462.
37 S. Fernández, U. Villanueva, A. de Diego, G. Arana and J. M. Madariaga, *J. Mar. Syst.*, 2008, **72**, 332-341.
38 D. N. Lumsden, *J. Sed. Petrol.*, 1979, **49**, 429-436.
39 J. H. Meyers, *J. Sed. Petrol.*, 1987, **57**, 558-570.

40 R. Ravisankar, E. Manikandan, M. Dheenathayalu, B. Rao, N. P. Seshadreesan and K. G. M. Nair, *Nucl. Instr. Meth. Phys. Res. B*, 2006, **251**, 496-500.
41 J. B. Teng and J. W. Shen, *Sci. China Ser. D*, 2008, **51**, 30-40.
42 O. Lopez, P. Zuddas and D. Faivre, *Geochim. Cosmochim. Act.*, 2009, **73**, 337-347.
43 U. Schreiber, R. Gademann, P. Bird, P. J. Ralph, A. W. D. Larkum and M. Kuehl, *J. Phycol.*, 2002, **38**, 125-134.
44 A. E. Adams and K. Schofield, *J. Sediment. Petrol.*, 1983, **53**, 417-421.
45 Y. Van Lith, R. Warthmann, C. Vasconcelos and J. A. Mckenzie, Geobiology, 2003, **1**, 71-79.
46 H. Yang, R. M. Hazen, R. T. Downs and L. W. Finger, *Phys. Chem. Miner.*, 1997, **24**, 510-519.
47 N. Y. Mostafa, A. A. Shaltout, M. S. Abdel-Aal and A. El-maghraby, *Mater. Design*, 2010, **31**, 3677-3682.
48 J. D. Milliman, M. Gastner and J. Muller, *Geol. Soc. Am. Bull.*, 1971, **82**, 573-580.
49 F. Zhang, H. Xu, K. Hironi and E. E Roden, *Am. Mineral.*, 2010, **95**, 1650-1656.
50 A. S. Khadkikar and C. Rajshekhar, Curr. Sci. India, 2003, **84**, 933-936.

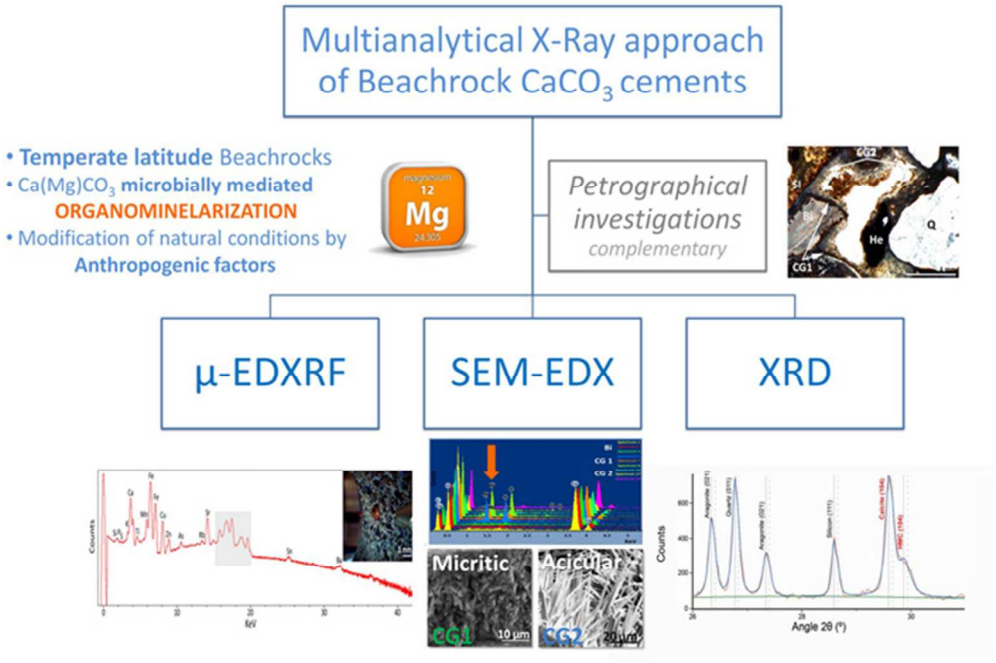

60x39mm (300 x 300 DPI)